Mon. Not. R. Astron. Soc. **399,** 1106–1118 (2009) doi:10.1111/j.1365-2966.2009.15197.x

The SDSS DR6 luminosity functions of galaxies

Antonio D. Montero-Dorta⋆ and Francisco Prada

Instituto de Astrofísica de Andalucía (CSIC), Granada, E-18008, Spain

Accepted 2009 June 2. Received 2009 June 1; in original form 2008 July 30

ABSTRACT

We present number counts, luminosity functions (LFs) and luminosity densities of galaxies obtained using the Sloan Digital Sky Survey Sixth Data Release (SDSS DR6) in all SDSS photometric bands. Thanks to the SDSS DR6, galaxy statistics have increased by a factor of $\sim$7 in the u band and by a factor between $\sim$3 and $\sim$5 in the rest of the SDSS bands with respect to the previous work of Blanton et al. In addition, we have ensured a high redshift completeness in our galaxy samples, mainly by minimizing the effect of brightness-dependent incompleteness. With these advances, we have estimated very accurate SDSS DR6 LFs at both the bright and the faint end. In the $^{0.1}r$ band, our LF is well fitted by a Schechter LF with parameters $\Phi_* = 0.93 \pm 0.07$, $M_* - 5\log_{10} h = -20.71 \pm 0.04$ and $\alpha = -1.26 \pm 0.02$. As compared with previous results, we find some notable differences. At the bright end of the $^{0.1}u$-band LF we find a remarkable excess, of $\sim$1.7 dex at $M_{^{0.1}u} \simeq -20.5$, with respect to the best-fitting Schechter LF. This excess weakens in the $^{0.1}g$ band, fading away towards the very red $^{0.1}z$ band. A preliminary analysis on the nature of this bright-end bump reveals that it is composed of quasi-stellar objects/type 1 Seyferts ($\sim$60 per cent), starbursts and star-forming galaxies ($\sim$20 per cent) and normal galaxies ($\sim$20 per cent). It seems, therefore, that an important fraction of this excess luminosity may come from nuclear activity. At the faint end of the SDSS DR6 LFs, where we can reach 0.5–1 mag deeper than the previous SDSS LF estimations, we obtain a steeper slope that increases from the $^{0.1}u$ band, with $\alpha = -1.05 \pm 0.05$, to the very red $^{0.1}z$ band, with $\alpha = -1.26 \pm 0.03$. We have also investigated the effect of galaxy evolution on our LFs. These state-of-the-art results may be used to constrain a variety of aspects of star formation histories and/or feedback processes in galaxy formation models.

Key words: catalogues – surveys – galaxies: luminosity function, mass function – large-scale structure of Universe.

1 INTRODUCTION

From the pioneering work of Humason (1956) and Sandage (1978), who measured redshifts of bright galaxies from the Shapley–Ames photometric catalogue (Shapley & Ames 1932), much effort has been invested in mapping the luminous and matter contents of the Universe. The Center for Astrophysics (CfA) Survey (Huchra et al. 1983) is considered as the first proper redshift survey, specifically designed for cosmology studies. More important, from the first slice of about 1000 galaxies, the CfA Redshift Survey (RS) provided the community with observational evidence of an old theoretical, and at times controversial idea: the existence of a large-scale structure of galaxies in the Universe (LSS; Davis et al. 1985). This first vision of cosmic complexity encouraged the development of new imaging and spectrometric technology and, consequently, gave rise to a number of other redshift surveys that followed different approaches and strategies. To name but a few, the Southern Sky Redshift Survey (SSRS; da Costa et al. 1988); the Perseus–Pisces catalogue (Giovanelli & Haynes 1991) or the catalogues based on data from the *Infrared Astronomical Satellite* (*IRAS*). In the last decade, the emergence of multifibre spectrographs set the scene for larger and deeper redshift surveys. Examples of these are the Las Campanas Redshift Survey (LCRS; Shectman et al. 1996), consisting of 26 418 galaxies with an average redshift of $z \sim 0.1$; or the 2 degree Field Galaxy Redshift Survey (2dFGRS; Colless et al. 2001), with about 222 000 galaxies and covering a sky area of 1500 deg^2. Finally, the Sloan Digital Sky Survey (SDSS; York et al. 2000) is the largest photometric and spectroscopic survey ever compiled, and represents the most accurate map of the nearby Universe at $z \lesssim 0.3$. The SDSS Sixth Data Release (DR6; Adelman-McCarthy et al. 2008), that we use in this paper, contains spectroscopic information

⋆E-mail: amdorta@iaa.es

for more than 1000 000 galaxies and quasars which spread over 7425 deg^2 on the sky. Only in recent years, with surveys like the DEEP2 Galaxy Redshift Survey (Davis et al. 2003) or the VIMOS-VLT Deep Survey (VVDS; Le Fevre et al. 2003), have we reached the stage where we can study the galaxy population in the distant ($z \sim 1$) Universe. Other high-z surveys are currently being completed.

The advances in the survey field also made it necessary to develop data reduction pipelines and analysis tools to process and understand increasingly larger data sets. These days, cosmologists use a number of statistics to characterize, for a particular survey, the distribution of galaxies in three-dimensional space. Number counts, selection functions, luminosity functions (LFs) or correlation functions are just a few examples. In this work we focus on the number counts and the LFs of galaxies, that are drawn from the SDSS DR6. Number counts, which describe the distribution of fluxes of galaxies, have been calculated for a number of surveys. The general consensus is that, in the close-by Universe, galaxy number counts look like what we expect from a Euclidean, non-evolving universe. Yasuda et al. (2001) obtained number counts for the SDSS commissioning data in all *ugriz* bands. Norberg et al. (2002) provided number counts for the 2dFGRS in the b_j band. Feulner et al. (2007) not only estimated galaxy number counts for a set of catalogues based on the Munich Near-Infrared Cluster Survey (MUNICS; Drory et al. 2001) but also presented a complete review of this subject in the literature (see their fig. 8). In contrast to galaxy number counts, the LF, which is the number density of galaxies per unit absolute magnitude, has been historically a rather controversial issue. For example, Marzke, Huchra & Geller (1994) – using the CfA RS –, Norberg et al. (2002) – 2dFGRS – and Blanton et al. (2003a) – SDSS DR2 – all obtained very different results.

Both the LF and the luminosity density of galaxies are observational signs of the process of galaxy formation and evolution. A precise determination of these statistics is needed to constrain current theories. Consequently, new discoveries in observational cosmology could make a strong impact in our understanding of the physical processes that drive the birth and life of galaxies in the Universe. Nowadays, state-of-the-art models of galaxy formation invoke a number of galactic 'mechanisms', which are connected through the so-called feedback processes. Disentangling these relations is an ambitious but crucial task in modern cosmology. In this sense, the semi-analytic models (SAMs) of galaxy formation (e.g. Croton et al. 2006), which are embedded in N-body simulations like the Millennium Run (see Springel et al. 2005), are a very useful tool for cosmologists. These SAMs are a good ground for testing new theoretical ideas and understanding their observational implications.

The main purpose of this work is to take advantage of the large increase in the galaxy statistics thanks to the SDSS DR6 to obtain the number counts, LFs and luminosity densities of galaxies in the nearby Universe. We intend to shed light both at the faint end of the LF, where most discrepancies come from, and at the bright end, where statistics have always been poor and errors, consequently large. In Section 2 we briefly describe the SDSS DR6, discuss our sample selection and comment on redshift completeness. In Section 3 we present our results on the number counts, the LFs and the luminosity densities of galaxies in each one of the SDSS photometric bands. Finally, in Section 4 we discuss our results and in Section 5 we present a summary of our work. Throughout this paper, unless otherwise stated, we assume a standard Λ cold dark matter (ΛCDM) concordance cosmology, with $\Omega_{\rm m} = 0.3$, $\Omega_\Lambda = 0.7$ and $h = 1$. In addition, we use AB magnitudes.

2 THE SLOAN DIGITAL SKY SURVEY DATA RELEASE 6: DATA SAMPLE SELECTION AND REDSHIFT COMPLETENESS

In this work, we use the SDSS DR6 (Adelman-McCarthy et al. 2008). This data set almost completes the North Galactic Cap, containing photometric information of ∼290 million objects over 9583 deg^2. Around 1.27 million objects were selected for spectroscopy, covering an area of 7425 deg^2 on the sky. Important for this work, spectroscopy is available for ∼900 000 galaxies down to magnitude $r \sim 17.77$ (York et al. 2000; Stoughton et al. 2002). Detailed information about the SDSS DR6 can be found in Adelman-McCarthy et al. (2008).

The SDSS DR6 is the largest spectroscopic survey of the nearby Universe publicly available. The SDSS collaboration have successively extended their catalogues since the times of the SDSS Early Data Release and, consequently, improved enormously our capability of mapping the Universe up to redshift $z \sim 0.25$. A few years ago, Blanton et al. (2003a) used the SDSS DR2 to estimate the LF of galaxies. In this work, thanks to the SDSS DR6, the size of our samples has risen by a factor of ∼7 in the very blue u band and by a factor of between ∼3 and ∼5 in the other bands (g, r, i and z). This huge enhancement in the statistics will be especially useful at the bright end of the LF, where the number density is lower. In addition, we expect to reach deeper magnitudes at the faint end with respect to previous works. Galaxy number counts can also be estimated with significantly more accuracy. It is therefore well justified to update the current knowledge on the number counts, LFs and luminosity densities of galaxies in the close-by Universe.

2.1 Data sample selection

We have drawn our samples from the NYU Value Added Galaxy Catalog (NYU-VAGC) DR6 (Blanton et al. 2005b). The NYU-VAGC is a compilation of galaxy catalogues cross-matched to the SDSS data products that includes a number of useful quantities derived from the photometric and the spectroscopic catalogues (such as K-corrections or absolute magnitudes). It also incorporates a precise and user-friendly description of the geometry of the survey.

Our parent sample (PS), which is the galaxy catalogue from which we extract all samples that we use in this paper, is built from the LSS sample of the NYU-VAGC and contains all galaxies that satisfy the criteria of the SDSS Main Galaxy Sample (Strauss et al. 2002) – except for those which are close to a saturated bright star. With these first restrictions the PS is composed of 947 053 galaxies that spread over 7280.35 deg^2 on the sky. From this catalogue, each sample is drawn by applying the following cuts to the redshift and the apparent magnitude:

(i) $m_{\rm min}(j) < m(j) < m_{\rm max}(j)$,
(ii) $z_{\rm min}(j) < z(j) < z_{\rm max}(j)$,

where $j = u, g, r, i, z$. We use extinction-corrected Petrosian magnitudes and heliocentric redshifts. In Table 1 we show lower and upper limits of these quantities along with the number of galaxies for each sample.

At this point, it is necessary to clarify the motivation for each cut. The apparent magnitude limits of Table 1 are set to ensure that the effect of redshift incompleteness is small in our SDSS galaxy samples. In a spectroscopic survey and strictly speaking, redshift completeness is defined as the fraction of galaxies with a reliable redshift estimation of all galaxies lying within the survey window and brighter than the survey apparent magnitude limit.

Table 1. Number of galaxies and limits in apparent magnitude and redshift of each SDSS photometric band sample. Motivation for each cut is discussed in Section 2.1. The slope in units of mag^{-1} of galaxy number counts (see Section 3.1) within the apparent magnitude and redshift limits of each sample is also provided. Within these ranges, number counts are consistent with a Euclidean, non-evolving universe.

Band	Number	$m_{\rm min}$	$m_{\rm max}$	$z_{\rm min}$	$z_{\rm max}$	Slope
u	153 411	16.45	18.81	0.020	0.170	0.615 ± 0.013
g	247 463	14.55	17.91	0.020	0.160	0.586 ± 0.009
r	437 565	13.93	17.6	0.020	0.220	0.591 ± 0.006
i	423 369	13.55	17.20	0.020	0.235	0.597 ± 0.007
z	378 833	13.40	16.87	0.020	0.24	0.604 ± 0.007

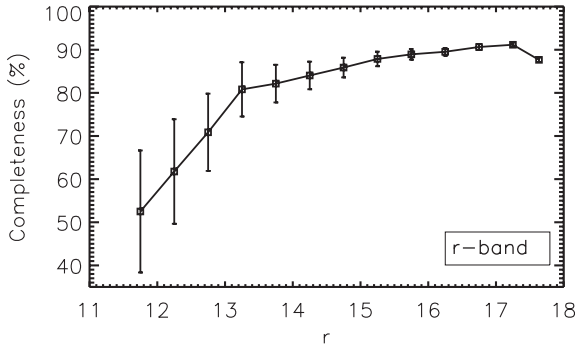

Figure 1. Redshift completeness versus apparent magnitude in the r band. At $r \lesssim 14$ completeness decreases sharply. Errors have been estimated by propagating the Poissonian uncertainties to the redshift completeness.

In practice, it is common to think of completeness as relative to the target population, i.e. to those galaxies that have been selected for spectroscopy from the photometric catalogue. Unless otherwise stated, this is the definition we will use throughout this paper. In the SDSS, brightness-dependent redshift incompleteness starts to be important at $r \lesssim 15$. This is clearly noticeable in Fig. 1, where we show redshift completeness as a function of r-band apparent magnitude (see Section 2.2 for further discussion). At the faint end, redshift incompleteness in all SDSS bands is dominated by the intrinsic faint limit of the Main Galaxy Sample (Strauss et al. 2002), i.e. $r = 17.77$. In order to set these limits, we have made use of the SDSS galaxy number counts, that will be properly discussed in Section 3.1. For each galaxy sample, we have taken the magnitude range where the number of galaxies rises at constant rate in each SDSS band, with a 0.1-dex deviation allowance (see Fig. 4, later, where galaxy number counts have been scaled by a Euclidean, non-evolving model). In the r band, we use a faint limit of $r = 17.6$, instead of $r = 17.77$. By restricting ourselves to this more conservative flux limit we can define a complete sample, avoiding some possible inconsistencies in the photometric calibration at $r > 17.6$ (see Blanton et al. 2001, for a detailed explanation). For consistency, in the rest of the SDSS bands we have ensured that the number of objects with $r > 17.6$ is less than 2 per cent. Within the apparent magnitude ranges of Table 1, we estimate that redshift completeness is ∼85 per cent in all SDSS bands. In Section 2.2, we will discuss on redshift incompleteness issues in the SDSS in more detail.

In Fig. 2, we show the redshift distribution for the PS in each SDSS photometric band. This figure illustrates the motivation for the redshift limits given in Table 1. The lower redshift limit is set to $z = 0.02$ to avoid the redshift incompleteness that affects the very

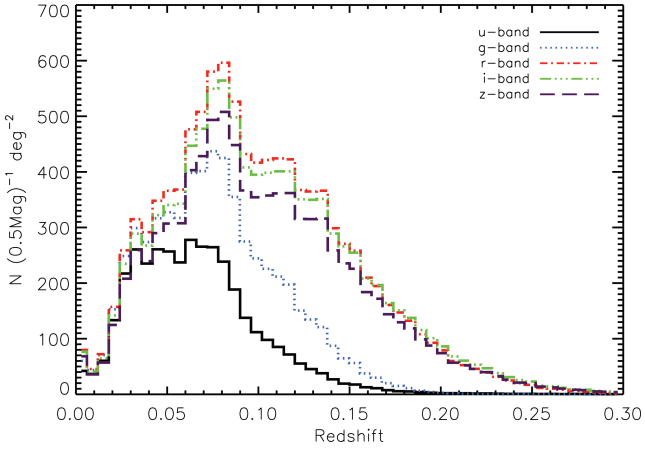

Figure 2. Redshift distributions in all SDSS photometric bands.

bright and nearby galaxies. The upper redshift limit corresponds to the redshift at which 98 per cent of objects are selected in each sample and is set for consistency.

2.2 Redshift completeness

It is well known that the brightest galaxies in the SDSS catalogues are affected by a severe redshift incompleteness. This effect is especially important for nearby galaxies. Apparently large and complex objects represent a major task for the photometric SDSS pipelines (Strauss et al. 2002). In order to illustrate this, we have cross-matched the SDSS DR5 and the Third Reference Catalog of Bright Galaxies (RC3; Corwin, Buta & de Vaucouleurs 1994), which is supposed to be reasonably complete for very bright and nearby galaxies ($r \lesssim 15$ and $z \lesssim 0.05$). We found that around 66.5 per cent of RC3 lying within the DR5 sky coverage, and therefore apparently imaged by the SDSS, have a corresponding object in the photometric catalogue. Moreover, only half of these photometric objects have a spectroscopic counterpart. Therefore, we estimate that the SDSS successfully gets the redshift of ∼1/3 of the very bright and large galaxies.

In addition, and affecting the entire magnitude range, is the so-called fibre collisions problem. This source of incompleteness, which is due to the fact that fibres cannot be placed closer than 55 arcsec, is responsible for most incompleteness in the SDSS data. Strauss et al. (2002) estimated that affects ∼6 per cent of all target galaxies.

In Fig. 1, we show how redshift completeness varies with apparent magnitude in the r band. At $r \simeq 14$, redshift completeness falls from ∼85 to ∼50 per cent at $r \simeq 12$. At the faint end, however, it reaches a plateau at 90 per cent – down to $r \simeq 17.8$ – which is in agreement with Strauss et al. (2002). In the rest of the SDSS bands, redshift completeness decreases not only at the bright end but also at the faint end. This is due to the intrinsic r-band faint limit of the Main Galaxy Sample at $r = 17.77$. Interestingly, the apparent magnitude, $m_{\rm max}(j)$, at which this decrease occurs varies between bands as a result of the dispersion in the colours of galaxies. We have checked that, by imposing $m_{\rm max}(j) > m(j) > m_{\rm min}(j)$, we ensure that each galaxy sample is approximately 85 per cent complete in any magnitude bin.

Another aspect of redshift completeness that should be carefully taken into account is its angular variation. In this paper we deal with number counts and LFs in the entire SDSS DR6 spectroscopic catalogue. These tasks require knowing the effective area

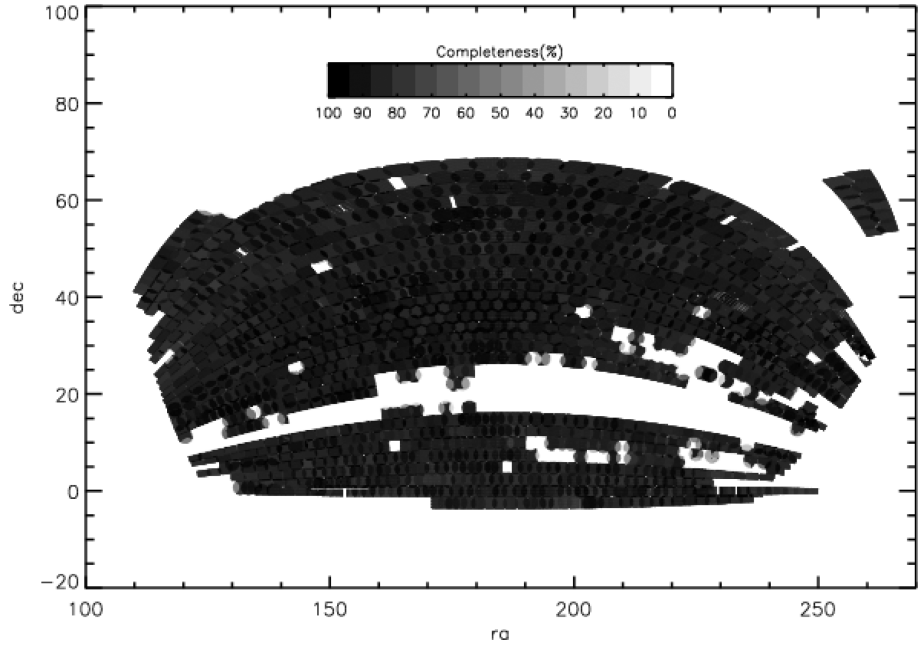

Figure 3. Angular redshift completeness of the SDSS DR6 spectroscopic catalogue in the right ascension range 110° < RA < 270°, which encompasses ∼99 per cent of the survey. Each polygon in the plot is an area of constant completeness. Polygons are also colour coded in white to black tones, meaning from 0 to 100 per cent completeness.

covered on the sky by the sample. The survey masks, available at the NYU-VAGC website, provide us with this information. However, redshift completeness is far from being uniform across the sky. In Fig. 3, we show the angular sky redshift completeness of the SDSS DR6 spectroscopic catalogue for a major part of the survey (∼99 per cent), just excluding objects outside the range 110° < RA < 270°, for the sake of clarity. The plot has been pixelized so that each pixel – or polygon – is an area of constant completeness. Polygons are also colour coded in white to black tones, the latter meaning 100 per cent completeness. Approximately 10 per cent of the total area is covered by polygons with less than 80 per cent completeness. In principle, by taking these regions into account we would be overestimating the area covered on the sky by our samples. However, since the main source of incompleteness in the SDSS, as discussed above, comes from the fibre spacing constraint, one would expect the majority of the low-completeness polygons to lie in highly dense regions on the sky. In order not to underrepresent these regions, we have not excluded incomplete polygons in our analysis. We have checked, however, that the exclusion of these polygons would not alter our results in any significant way.

Finally, we cannot discard the possibility that the SDSS spectroscopic catalogue is incomplete for very low surface brightness objects, i.e. $\mu_{r,50} \gtrsim 24$ (see Strauss et al. 2002). The presence of this selection effect in the data could in principle affect our results. However, we have evidence that the surface brightness of most galaxies in the SDSS, and consequently in our galaxy samples, is far greater than $\mu_{r,50} \simeq 24$ (Blanton et al. 2003a, 2005a).

3 RESULTS

3.1 Number counts

In Fig. 4 we plot with different symbols the logarithm of the number of galaxies per unit area and apparent magnitude (actually, half magnitude), scaled by a Euclidean model for all SDSS bands. We

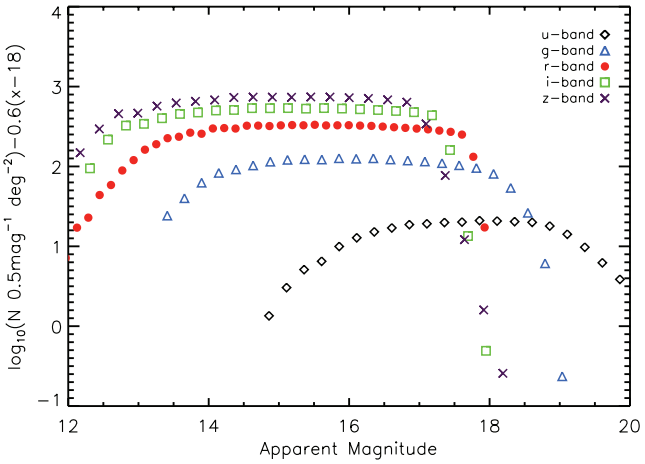

Figure 4. Galaxy number counts in all SDSS bands scaled by a Euclidean model in bins of half a magnitude. Poissonian errors are of similar size as symbols, so they are not shown.

choose, arbitrarily, the following model for Euclidean counts:

$$N_{\rm Euclidean} = 10^{0.6(x-18)}, \quad (1)$$

where x represents the apparent magnitude in each SDSS band.

In the r band, galaxy number counts increase by a factor of about 10 from $r \sim 12$ to ∼13.5. This magnitude range is strongly affected by redshift incompleteness, as discussed above (see also Fig. 1). From $r \sim 14$ to ∼18, counts rise at approximately the same rate as that of the model (equation 1). At $r \sim 18$, where the SDSS spectroscopic faint-end limit is set ($r = 17.77$), galaxy number counts fall sharply.

In the rest of the bands, the behaviour is very similar at the bright end and is also due to redshift incompleteness. In the z band, counts start to follow the Euclidean model at $z \sim 13.5$. In the i band, this happens at $i \sim 13.5$; in the g band, at $g \sim 14.5$ and in the

u band, at $u \sim 16.5$. At the faint end, galaxy number counts fall roughly at $u \sim 19, g \sim 18, i \sim 17$ and $z \sim 17$ (see Table 1 for more accurate values). This decrease is obviously less pronounced than in the r band, due to the different colours of galaxies. In addition, the slope of this faint-end decrease in the galaxy number counts is considerably steeper in the red bands than it is in the bluer bands. This is due to the fact that the dispersion in the $(u - r)$ colours in notably larger than that of the $(r - z)$ colours (Blanton et al. 2003b).

Number counts are consistent with a Euclidean, non-evolving universe in all SDSS bands within the magnitude and redshift ranges given in Table 1. Within these ranges, the slopes in units of mag^{-1} of the SDSS DR6 galaxy number counts are also listed in this table. Note that the small deviations that we find with respect to the Euclidean model are probably due to the presence of the LSS.

Our results for the nearby Universe are in agreement with a number of previous works (see Feulner et al. 2007 for a review). However, only Yasuda et al. (2001) presented galaxy number counts obtained using the SDSS. The authors used imaging data taken only during the commissioning phase. They found a Euclidean-like behaviour up to magnitude $m_{\rm min} \sim 12$ – except for the u band, where $m_{\rm min} \sim 14$ – (see their fig. 8). The lack of galaxies at the very bright end of Fig. 4 with respect to photometric number counts from Yasuda et al. (2001) is partially due to the strong redshift incompleteness that affects the SDSS spectroscopic catalogue in these magnitude ranges (see Section 2.2). However, our results and those from Yasuda et al. (2001) are not directly comparable. First, they used a very limited sample, in terms of sky coverage ($\sim$230 deg^2). Secondly, comparing spectroscopic and photometric results is always tricky.

3.2 Luminosity functions

In order to estimate the LF of galaxies in each SDSS photometric band, we take absolute magnitudes and K-corrections from the NYU-VAGC DR6 LSS catalogue. Following Blanton et al. (2003a), absolute magnitudes are calculated with the SDSS photometric bands shifted to $z = 0.1$. With this convention, the absolute magnitude of a galaxy in a given band shifted to $z = 0.1$, $M_{0.1j}$, would be constructed from its apparent magnitude at $z = 0$, m_j and its redshift z as follows:

$$M_{0.1j} = m_j - 5\log_{10} h - {\rm DM}(z) - K_{0.1j}(z), \qquad (2)$$

where DM(z) is the distance modulus (which depends also on the cosmological parameters) and $K_{0.1j}(z)$, the K-correction for the galaxy in the shifted band $^{0.1}j$. Blanton et al. (2003a) included another correction in expression (2) to account for the evolution of the luminosity of a galaxy from redshift z to $z = 0.1$, the so-called evolution correction. Other authors have tried to implement a similar correction using different approaches (i.e. Norberg et al. 2002, for the 2dFGRS). It seems tempting to think, however, that this correction should be very small within the redshift ranges we use here. As this refinement is still subject to large uncertainties, we have opted to present uncorrected LFs and devote Section 3.2.1 to discussing the effect of evolution on our LFs.

In Fig. 5, we show the distribution of K-corrected absolute magnitudes in each galaxy sample. The shape of the absolute magnitude distribution is very similar in all SDSS bands: a Gaussian-like distribution slightly skewed to fainter magnitudes. However, mean values move towards bright-end bins from $^{0.1}u$ band – $M_{0.1u} \sim -18$ – to $^{0.1}z$ band – $M_{0.1z} \sim -21.5$, which is consistent with the fact that red objects are, on average, brighter than blue objects. In Fig. 6, we also show the bimodal $^{0.1}u - {}^{0.1}r$ colour distribution of galaxies in our

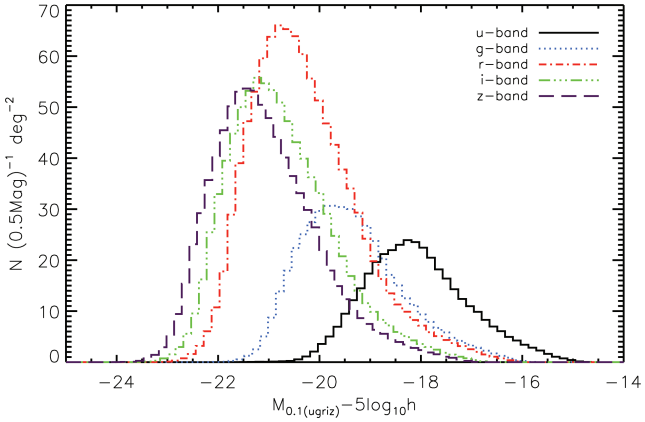

Figure 5. Absolute magnitude distribution in each sample. Although the shape of the distributions is very similar, mean values move towards bright-end magnitude bins from $^{0.1}u$ band to $^{0.1}z$ band, as red objects are, on average, brighter than blue objects.

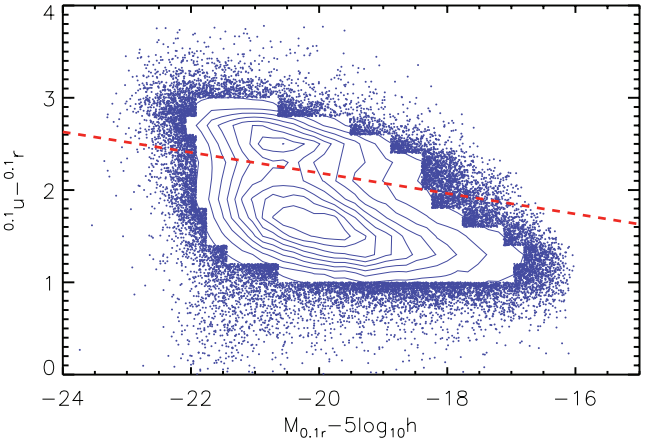

Figure 6. The $(^{0.1}u - {}^{0.1}r)$ CMD in the $^{0.1}r$ band. The dashed line represents the demarcation commonly used to separate red and blue galaxies.

$^{0.1}r$-band sample. With a dashed line we represent the demarcation commonly used to separate red and blue objects (see Strateva et al. 2001).

We use the Stepwise Maximum Likelihood Method (SWML; Efstathiou, Ellis & Peterson 1988) to estimate the LF of galaxies, that is commonly expressed in the literature as $\Phi(L)$. This technique does not rely on any assumption about the shape of $\Phi(L)$ and is considered as the most reliable estimator of the LF. For more details about this method see Efstathiou et al. (1988) and Norberg et al. (2002). The SWML requires an independent estimation of the number density of galaxies, i.e. the normalization constant, n. We use the following prescription proposed by Davis & Huchra (1982) based on the selection function of each galaxy, $\phi(z_i)$, and the maximum volume encompassed by the sample, $V_{\rm max}$:

$$n = \frac{1}{V_{\rm max}} \sum_i \frac{1}{\phi(z_i)}. \qquad (3)$$

In Fig. 7 we show the SWML estimate of the SDSS DR6 LF in the $^{0.1}r$ band. In addition, we overplot with a dashed line the best-fitting Schechter function (Schechter 1976), which has the following

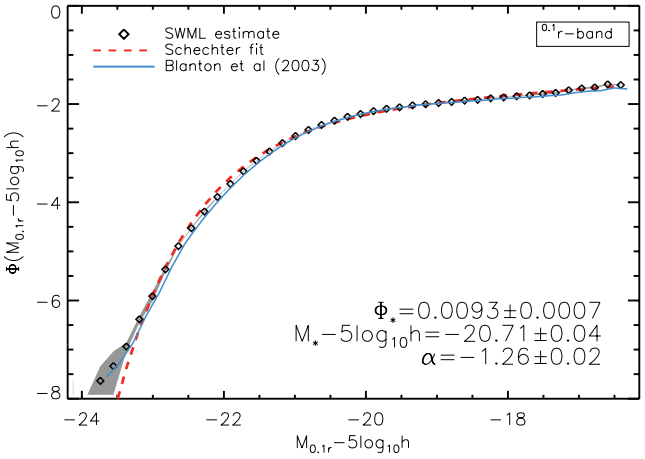

Figure 7. The $^{0.1}r$-band SDSS DR6 LF. The SWML LF estimate is shown in diamonds. The dashed line represents the best-fitting Schechter function and the solid line, the $^{0.1}r$-band LF from Blanton et al. (2003a). Best-fitting values of Schechter parameters α, M_* and Φ_* are also shown in the figure. Shaded regions represent the 1σ uncertainty calculated using a bootstrapping technique.

Table 2. Values of Schechter parameters α, M_* and Φ_* of the best-fitting Schechter function in all SDSS bands for this work and for Blanton et al. (2003a). Note that it is not convenient to compare LFs by just looking at their best-fitting Schechter parameters. Also bear in mind that both estimates are not strictly comparable, due to differences in the sample selection, the treatment of galaxy evolution and, especially, the size of the samples. In Sections 3.2.1 and 4 we discuss the importance of these inconsistencies.

This work			
Band	$\Phi_*(10^{-2}\,h^3\,\mathrm{Mpc}^{-3})$	$M_* - 5\log_{10}h$	α
$^{0.1}u$	4.95 ± 0.27	-17.72 ± 0.07	-1.05 ± 0.05
$^{0.1}g$	1.25 ± 0.10	-19.53 ± 0.04	-1.10 ± 0.03
$^{0.1}r$	0.93 ± 0.07	-20.71 ± 0.04	-1.26 ± 0.02
$^{0.1}i$	1.14 ± 0.11	-20.93 ± 0.05	-1.14 ± 0.03
$^{0.1}z$	0.93 ± 0.09	-21.40 ± 0.05	-1.26 ± 0.03
Blanton et al. (2003)			
Band	$\Phi_*(10^{-2}\,h^3\,\mathrm{Mpc}^{-3})$	$M_* - 5\log_{10}h$	α
$^{0.1}u$	3.05 ± 0.33	-17.93 ± 0.03	-0.92 ± 0.07
$^{0.1}g$	2.18 ± 0.08	-19.39 ± 0.02	-0.89 ± 0.03
$^{0.1}r$	1.49 ± 0.04	-20.44 ± 0.01	-1.05 ± 0.01
$^{0.1}i$	1.47 ± 0.04	-20.82 ± 0.02	-1.00 ± 0.02
$^{0.1}z$	1.35 ± 0.04	-21.18 ± 0.02	-1.08 ± 0.02

shape:

$$\Phi(M) = 0.4\log(10)\Phi_* 10^{-0.4(M-M_*)(\alpha+1)} \times \exp[-10^{-0.4(M-M_*)}], \quad (4)$$

where α, M_* and Φ_* are the three parameters to fit. Values of these parameters for the best-fitting Schechter function are given in Table 2. For comparison, we also show in Fig. 7 the LF of Blanton et al. (2003a) with a solid line. This comparison will be addressed in the Discussion section. To calculate errors in the SWML estimates of the LF we perform a bootstrapping analysis using 1000 random subsamples of 1/3 of the number of objects in each sample. In Fig. 7, shaded regions represent the 1σ uncertainty obtained from this method.

Because of the big number statistics that we have, with about 450 000 galaxies in the $^{0.1}r$ band, errors are only significant at the very bright end of the LF. At the faint end, we can go down to $M_{0.1_r} \sim -16.5$, which means that we can build the LF with unprecedented precision within a very large range of magnitudes. As we will see below, the above statements hold for all SDSS bands. Our $^{0.1}r$-band LF is reasonably well fitted by a Schechter LF with a faint-end slope $\alpha = -1.26$. It is only at the very bright end where this best-fitting Schechter LF starts to underestimate our LF. At $M_{0.1_r} \lesssim -23.5$, statistics are poor and errors become increasingly large.

In Fig. 8 we present, in the same way as in Fig. 7, SWML estimates of the LF in bands $^{0.1}u$,$^{0.1}g$,$^{0.1}i$ and $^{0.1}z$, as well as their corresponding best-fitting Schechter LF. Values of best-fitting Schechter parameters are also given in Table 2. As in the $^{0.1}r$ band, errors are only significant at the very bright end of the $^{0.1}u$,$^{0.1}g$,$^{0.1}i$ and $^{0.1}z$ band LFs. In addition, we can go down to very faint magnitudes without losing precision.

In the very blue $^{0.1}u$ band, the shape of our SDSS DR6 LF is consistent with a Schechter LF with a slightly positive faint-end slope (corresponding to $\alpha = -1.05$). However, at the bright end, we find a remarkable luminosity excess with respect to the best-fitting Schechter LF. This excess, of $\sim$1.7 dex at $M_{0.1_u} \simeq -20.5$, is very significant within the magnitude range $-20.5 < M_{0.1_u} \lesssim -22$. In the $^{0.1}g$ band, this bright-end bump (BEB) weakens considerably, but it is probably still significant, even though errors are large according to our bootstrapping analysis. In this band, our SDSS LF is very well fitted by a Schechter LF with a positive faint-end slope, corresponding to $\alpha = -1.10$. Only at the very bright end, where the excess is still noticeable, do we find some discrepancy. Below, we provide a preliminary analysis and discussion on the nature of this bump at the bright end of the $^{0.1}u$-band LF, that may have important implications in terms of galaxy formation and evolution.

In the redder bands we find a positive faint-end slope, corresponding to $\alpha = -1.14$ in the $^{0.1}i$ band and $\alpha = -1.26$ in the $^{0.1}z$ band. The BEB has diminished but is still clearly significant in the $^{0.1}i$ band and only disappears completely in the very red $^{0.1}z$ band. It is interesting to note that, from the $^{0.1}u$ band to the $^{0.1}z$ band, the shape of the SWML estimate of the SDSS LF changes following a clear pattern. The faint-end slope increases towards the redder bands (see Table 2), being almost flat in the $^{0.1}u$ band and remarkably steep in the $^{0.1}z$ band. In this sense, the $^{0.1}r$-band SDSS LF seems to slightly deviate from this trend. At the faint end, we find a slope that is a bit larger than we could expect ($\alpha = -1.26$), but this could be just a consequence of the fact that the entire SDSS spectroscopic sample was selected in this band.

The BEB that shows up clearly in the $^{0.1}u$-band LF, and partially in the $^{0.1}g$-band and $^{0.1}i$-band LFs, is an interesting discovery that may have implications for our understanding of galaxy formation and evolution. In order to investigate the nature of the objects that populate it, we have selected all galaxies brighter than -20.5 in the $^{0.1}u$-band sample. We will hereafter refer to this population as BEB galaxies and to their corresponding sample, which is composed of 252 objects, as the bright-end bump sample (BEBS). It is convenient to remind that, although here we focus on the $^{0.1}u$ band, significant bright-end excesses have been found in both the $^{0.1}g$ band and the $^{0.1}i$ band. It is in the very blue $^{0.1}u$ band, however, were this population stands out more prominently.

We have visually inspected the spectra of all galaxies in the BEBS. In addition, we have taken the spectral classification of each individual galaxy, based on emission line ratios, from the NYU-VAGC. According to this analysis, about 60 per cent of objects have a typical quasi-stellar object (QSO) or type 1 Seyfert spectrum, $\sim$8 per cent of sources are classified as starburst galaxies (SBs), $\sim$12 per cent as star-forming galaxies (SFs) and

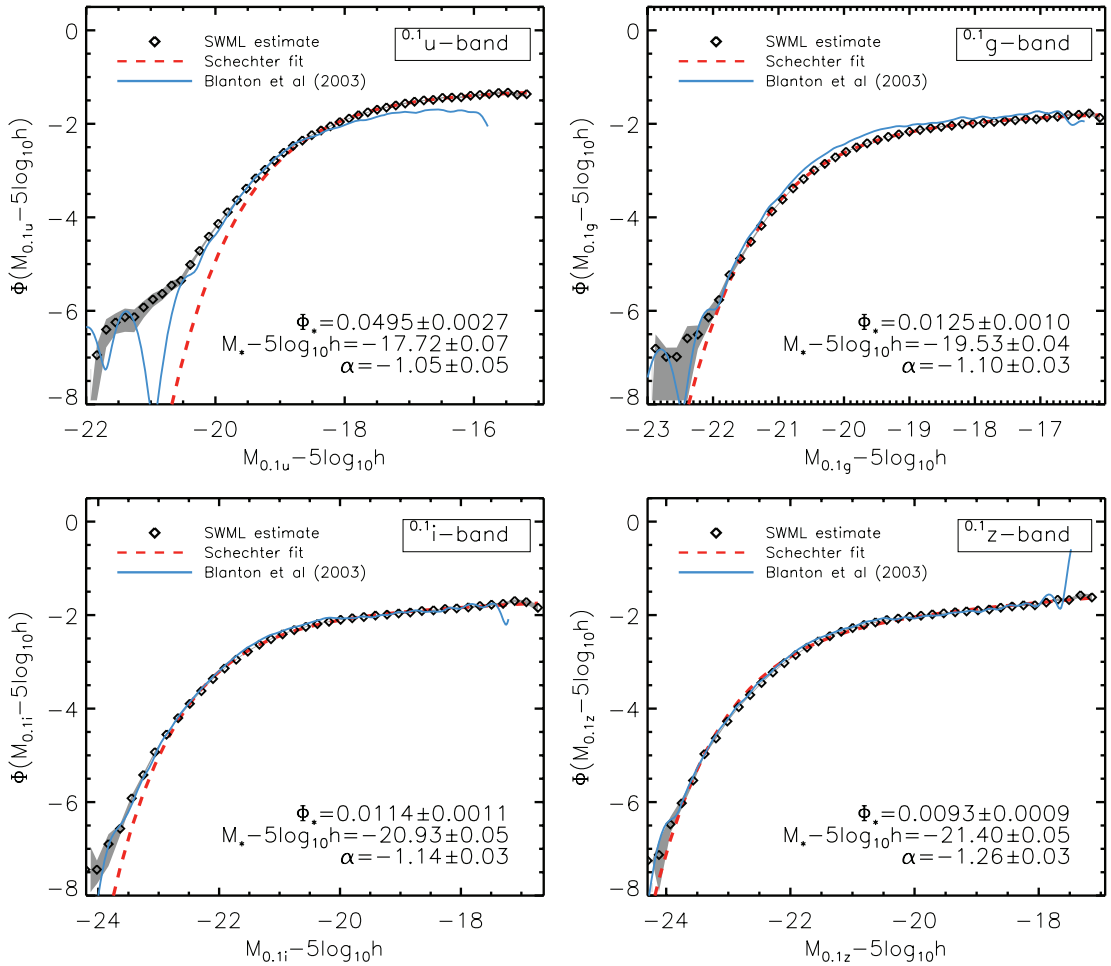

Figure 8. The SDSS DR6 LFs in bands $^{0.1}u$, $^{0.1}g$, $^{0.1}i$ and $^{0.1}z$. SWML LF estimates are shown in diamonds and best-fitting Schechter functions are represented by dashed lines. In addition, we overplot in each panel the LF from Blanton et al. (2003a). Best-fitting values of Schechter parameters α, M_* and Φ_* are also shown. Shaded regions represent the 1σ uncertainty calculated using a bootstrapping technique.

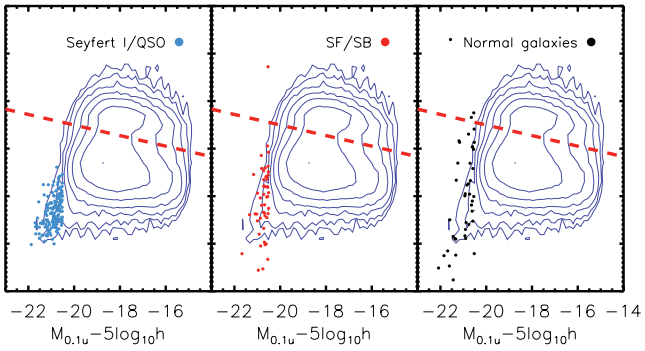

Figure 9. The $(^{0.1}u - {}^{0.1}r)$ versus $M_{0.1_u}$ color–magnitude diagram for the three types of BEB galaxies considered: QSOs/type 1 Seyferts (left-hand plot), SFs/SBs (middle plot) and normal galaxies (right-hand plot). The underlying CMD of the entire $^{0.1}u$-band sample from which BEB galaxies are selected is shown with log-spaced contours.

∼20 per cent of objects are normal galaxies that show no significant emission lines in their spectra. We hereafter consider three types of BEBS galaxies: QSOs/type 1 Seyferts (∼60 per cent), SBs/SFs (∼20 per cent) and normal galaxies (∼20 per cent). In Fig. 9 we plot in the $(^{0.1}u - {}^{0.1}r)$ versus $M_{0.1_u}$ colour–magnitude diagram (CMD) of the $^{0.1}u$-band sample the three types of BEB galaxies discussed above. In general, these galaxies form a relatively tight sequence at the bright end of the CMD, showing a considerable colour dispersion. Note that, in contrast to Fig. 6, density contours are now log-spaced and hence, these objects occupy an extremely underpopulated region in the CMD. In the left-hand plot, QSOs/type 1 Seyferts show the smallest colour dispersion and are, on average, the bluest: $\langle(^{0.1}u - {}^{0.1}r)\rangle = 0.68$. Both SFs/SBs (middle plot) and normal galaxies (right-hand plot) show much larger colour dispersion and are, on average, considerably redder, with $\langle(^{0.1}u - {}^{0.1}r)\rangle = 0.89$ and $\langle(^{0.1}u - {}^{0.1}r)\rangle = 0.99$, respectively. In the $^{0.1}u$ band, QSOs/type 1 Seyferts and normal galaxies are, on average, the brightest among the BEB galaxies: $\langle M_{0.1_u}\rangle = (-20.91^{\rm QSO/S1}, -20.75^{\rm SFs/SBs}, -20.99^{\rm normal})$.

We have checked that BEB galaxies are typically at high redshift relative to the average redshift of the $^{0.1}u$-band sample from which they are drawn. The mean redshift in the BEBS is $\langle z\rangle \sim 0.155$ while in the entire $^{0.1}u$-band sample is $\langle z\rangle \sim 0.080$. Note that the redshift limit of $z < 0.17$ that we have imposed for consistency in the $^{0.1}u$-band sample turns out to be slightly restrictive for the BEB galaxies, according to their redshift distribution. However, the above results remain unchanged as far as the mean properties of the BEB galaxies are concerned, when we extend this limit to $z \sim 0.2$. The size of the BEBS would increase to ∼1000 objects, though.

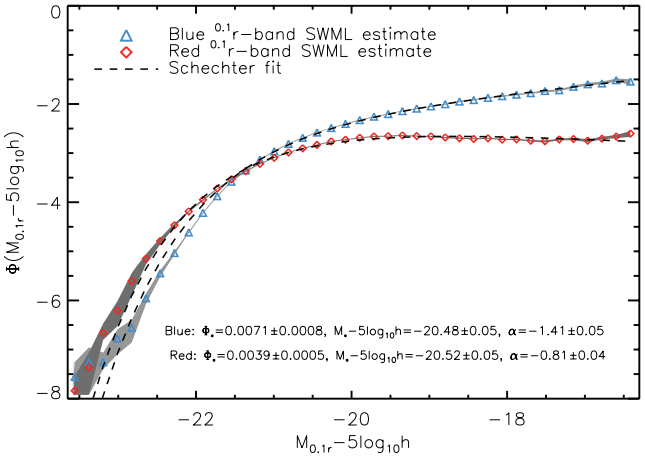

Figure 10. The $^{0.1}r$-band SDSS DR6 LF for blue and red galaxies separately. The SWML LF estimates are shown in diamonds. The dashed lines represents the best-fitting Schechter function. Best-fitting values of Schechter parameters α, M_* and Φ_* for both blue and red galaxies are also shown in the figure. Shaded regions represent the 1σ uncertainty calculated using a bootstrapping technique.

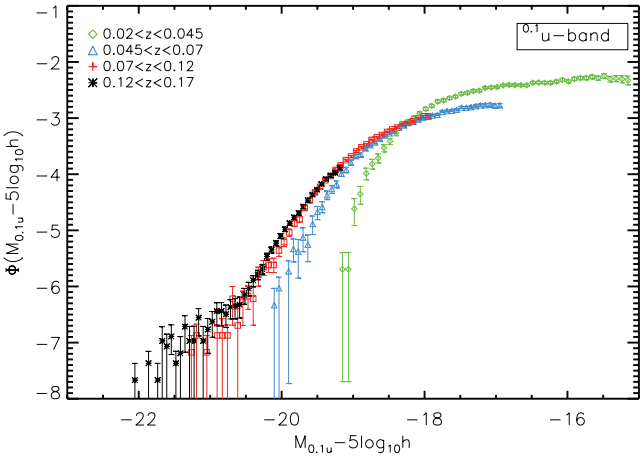

Figure 11. The evolution of the $^{0.1}u$-band LF in four redshift slices. Errors bars represent the 1σ uncertainty calculated using a bootstrapping technique. The number of objects in each redshift bin is listed in Table 3.

At this point, it is necessary to remark that this is a preliminary analysis. We have performed a rough classification of the BEB galaxies, and this is still subject to some uncertainty. However, our aim is to provide a first approach to the nature of this population of objects. In Section 4 we speculate on possible implications of these results.

Finally, in Fig. 10, we present, in the same way as in Figs 7 and 8, SWML estimates of the SDSS $^{0.1}r$-band LF for blue and red galaxies separately, as well as their corresponding best-fitting Schechter LF. Values of best-fitting Schechter parameters are also shown in the figure. The demarcation that we use to separate blue and red objects is represented by a dashed line in Fig. 6. The SDSS $^{0.1}r$-band LF of blue galaxies is well fitted by a Schechter LF with $\alpha = -1.41$. In contrast, the SDSS $^{0.1}r$-band LF of red galaxies has a negative faint-end slope, corresponding with $\alpha = -0.81$. At the bright end, at $M_{0.1r} \lesssim -21.5$, the blue LF falls remarkably below the red LF.

3.2.1 The effect of galaxy evolution

In previous sections, we assumed that the evolution in the luminosity of galaxies within the redshift intervals considered had a negligible effect on the SDSS LFs. This idea is based on the little redshift depth of our samples ($z \lesssim 0.2$). In this section, we elaborate on the validity of such an assumption. Accounting for galaxy evolution is, nevertheless, a rather difficult task. In principle, one should expect that different types of galaxies evolve with time in different ways. The evolutionary path of an average galaxy of a given type not only depends on intrinsic properties such as mass but also on the environment, with a number of possible processes being proposed (i.e. merger events, harassment, etc.). Unfortunately, our knowledge of these and other processes involved in a galaxy's evolution seems insufficient to treat this problem in an accurate way. Some previous works, however, have tried to account for evolution in a simple way, using different approaches. Blanton et al. (2003a) implemented a correction based on the change in the absolute magnitude distribution with redshift (Blanton, private communication). This correction ranges from $\sim$−0.15 mag for objects at $z \sim 0$ to +0.2 mag for galaxies at $z \sim 0.2$ and is responsible, according to this study, for the flattening of the faint-end slopes of their LFs. On the other hand, Norberg et al. (2002) used four different evolution corrections depending on the spectral type of the galaxy to calculate the b_j-band LF for the 2dFGRS. Even after applying this correction, they find a LF in the b_j band (which is roughly comparable to our SDSS $^{0.1}g$ band) with a remarkably steep faint-end slope, corresponding to $\alpha \sim -1.2$. Although efforts like these are extremely valuable and contribute to the understanding of the effect of evolution on the LF of galaxies, the approximations they use are still subject to major uncertainties. These uncertainties, which derive from our still limited knowledge of the process of galaxy evolution itself, become especially significant when dealing with relatively narrow redshift ranges, like those we use in this work.

In this work, we use a different approach and we investigate the evolution of the LF by binning our galaxy samples by redshift. The aim of this section is to show that accounting for evolution is not likely to alter, in any significant way, our main results, i.e. the prominent bright-end excess in the $^{0.1}u$-band LF and the relatively steep faint-end slopes in all SDSS bands. For the sake of simplicity, we will address this question by studying the evolution of the $^{0.1}u$-band and the $^{0.1}r$-band LFs.

In Fig. 11 we plot the $^{0.1}u$-band LF in four different redshift bins. The slicing has been designed to ensure that the number of objects is similar in the first three redshift bins and enough to guarantee a reliable estimation of the LF in the more distant one. The number of galaxies in each slice is listed in Table 3. Interestingly, we find that the $^{0.1}u$-band LF moves towards brighter magnitudes with redshift. The BEB appears only in the more distant slices, at $z > 0.10$. The bright-end incompleteness of the SDSS makes it difficult to know if this is just a selection effect (as the sampling volume is smaller at lower redshift) or a natural property of this population of galaxies. In the redshift interval $0.12 < z < 0.17$, the BEB stands up clearly. It is important to stress that by narrowing our redshift ranges we minimize the effect of evolution. Fig. 11 proves the presence of a prominent bright-end excess in the $^{0.1}u$-band LF at $z \sim 0.15$. We could expect a standard evolution correction (as those cited above) to produce mainly a small horizontal shift of the BEB towards fainter magnitudes in the $z = 0.1$ $^{0.1}u$-band LF of Fig. 8, but not the suppression of the excess. In fact, the existence of the BEB can be somehow inferred from previous works. Although noisy, clear signs of a bright-end excess can be found in the $^{0.1}u$-band and the $^{0.1}g$-band LFs of Blanton et al. (2003a) (see Fig. 8). Similarly,

Table 3. Number of galaxies in each redshift slice of the $^{0.1}u$-band and the $^{0.1}r$-band sample, corresponding to the evolution plots of Figs 11 and 12, respectively.

$^{0.1}u$ band	
Redshift bin	Number
$0.02 < z < 0.045$	40 738
$0.045 < z < 0.07$	46 310
$0.07 < z < 0.12$	54 843
$0.12 < z < 0.17$	9 737
$^{0.1}r$ band	
Redshift bin	Number
$0.02 < z < 0.07$	124 608
$0.07 < z < 0.11$	142 183
$0.11 < z < 0.15$	102 871
$0.15 < z < 0.22$	66 070

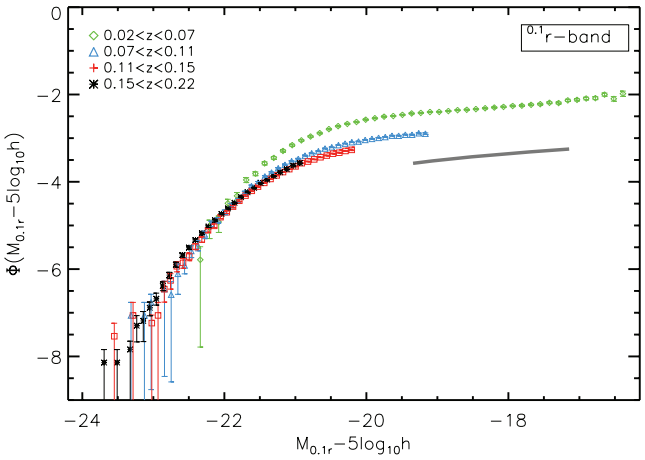

Figure 12. The evolution of the $^{0.1}r$-band LF in four redshift slices. Errors bars represent the 1σ uncertainty calculated using a bootstrapping technique. The number of objects in each redshift bin is listed in Table 3. The solid line represents a faint-end slope corresponding to $\alpha = -1.26$.

an statistically significant bright-end deviation from the best-fitting Schechter LF is obtained, although not reported, in the b_j-band LF of Norberg et al. (2002).

In Fig. 12 we present, in the same format as in Fig. 11, the evolution of the $^{0.1}r$-band LF. As Fig. 12 clearly shows, the faint end of the SDSS LF is almost exclusively determined by low-redshift galaxies ($z \lesssim 0.07$). At higher redshifts the SDSS is not deep enough to capture the faint objects. The faint-end slope that we obtain in the first redshift bin ($0.02 < z < 0.07$) is absolutely consistent with that of the $z = 0.1$ $^{0.1}r$-band LF of Fig. 8. To illustrate this, a solid line with a slope corresponding to $\alpha = -1.26$ has been plotted. A similar argument as that invoked to show that accounting for evolution could not produce the suppression of the BEB can be used here. As the faint-end slope of the LF is almost entirely determined by a narrow redshift range, it is unlikely that a realistic evolution correction could change this slope significantly. This assumption is in agreement with the theoretical work of Khochfar et al. (2007), where the evolution of the faint-end slope of the LF is investigated using SAMs of galaxy formation. The authors report a very small variation of α at low redshift, being less than 1 per cent between $z = 0.02$ and 0.10.

To summarize, although allowing for galaxy evolution in our galaxy samples in a proper way could produce slight adjustments to our LFs (that could even translate into small variations in the very sensitive best-fitting Schechter parameters, mainly in M_*), it seems unlikely, as we have shown above, that this correction could produce a qualitative alteration of our main results. In any case, it is still convenient not to forget the issue of evolution when comparing our best-fitting Schechter parameters with those from Blanton et al. (2003a). However, in Section 4 we discuss other inconsistencies between both works that are more likely to be responsible for the discrepancies we find.

3.2.2 *Petrosian magnitudes versus model magnitudes*

Petrosian magnitudes have widely been used in previous SDSS LF works. These are based on a modified form of the Petrosian (1976) system, measuring galaxy fluxes within a circular aperture whose radius is defined by the shape of the azimuthally averaged light profile. However, apparent magnitudes are estimated in other ways in the SDSS, each way being appropriate for a different type of science. In particular, model magnitudes, which are calculated by fitting an exponential or a de Vaucouleurs light profile, are also regarded as a reliable estimate of the flux of a galaxy. These magnitudes have the advantage of measuring almost unbiased colours of galaxies. In Fig. 13 we show the scatter between these two different flux estimates. In the right-hand plot, the r-band scatter is presented as a function of Petrosian apparent magnitude. As seen in this plot, the scatter increases towards fainter magnitudes in this band. Throughout the entire range, Petrosian magnitudes measure less flux on average than model magnitudes. At the fainter end, this loss can translate into as much as 0.5 mag. The cummulative distributions of the scatter in bands u, r and z are shown in the left-hand plot of Fig. 13. We have excluded the distributions in bands g and i for the sake of clarity. This plot shows that Petrosian magnitudes are increasingly fainter with respect to model magnitudes as we move to redder bands. In the very blue u band, however, the scatter is much larger than in the rest of the bands, ranging from -1 to 0.5 mag at the fainter end. Below, we address the question of how the choice of model magnitudes over the more conventional Petrosian magnitudes would affect our LF estimates.

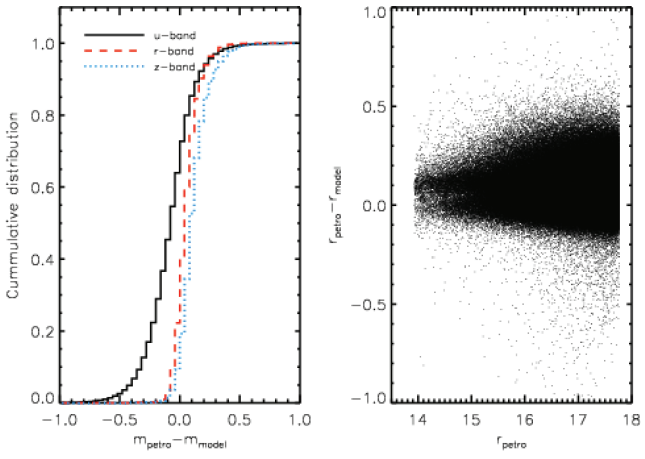

Figure 13. The scatter between Petrosian and model magnitudes. In the left-hand plot, the cummulative distribution of the scatter is shown in bands u, r and z. The distributions in bands g and i have been excluded for the sake of clarity. In the right-hand plot, we show the r-band scatter as a function of Petrosian apparent magnitude.

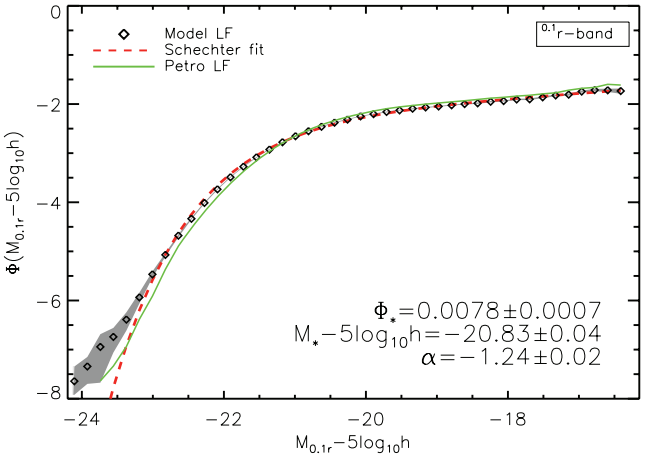

Figure 14. The $^{0.1}r$-band SDSS DR6 LF estimated using model magnitudes. The SWML LF estimate is shown in diamonds. The dashed line represents the best-fitting Schechter function and the solid line, the $^{0.1}r$-band SDSS DR6 LF estimated using Petrosian magnitudes. Best-fitting values of Schechter parameters α, M_* and Φ_* are also shown in the figure. Shaded regions represent the 1σ uncertainty calculated using a bootstrapping technique.

In order to be consistent in our comparison, we have followed a similar selection scheme as that discussed in Section 2.1. In addition, absolute magnitudes have been calculated in the same way as in equation (2) and K-corrections for model magnitudes have been taken from the NYU-VAGC. In Fig. 14 we present, in the format used throughout the paper, the SWML estimate of the SDSS DR6 LF in the $^{0.1}r$ band, obtained using model magnitudes. Instead of showing the LF of Blanton et al. (2003a) and in order to facilitate the comparison, we have overplotted our SDSS DR6 LF obtained using Petrosian magnitudes. In the same way we show, in Fig. 15, SWML estimates of the SDSS DR6 LF for model magnitudes in bands $^{0.1}u$, $^{0.1}g$, $^{0.1}i$ and $^{0.1}z$. Selection limits for the new samples and values of best-fitting Schechter parameters for the model LFs in all bands are listed in Table 4.

As seen in Figs 14 and 15, the scatter between Petrosian and model magnitudes has a noticeable impact on the LF. In the $^{0.1}u$ band, the LF is shifted downwards at the faint end, where the slope also flattens slightly: $\alpha = -1.00$ for the model LF and $\alpha = -1.05$ for the Petrosian LF. In contrast, in the rest of the photometric bands, the main difference is that the model LF is horizontally shifted to the bright end with respect to the Petrosian LF. The separation between both LFs is tightly related to the variation of M_*. Interestingly, this variation tends to increase towards the redder bands, reaching a value of ∼0.2 mag in the $^{0.1}i$ band and ∼0.12 in the very red $^{0.1}z$ band. This pattern is clearly consistent with the scatter in each band.

Note that some of the differences discussed above might be due, not only to the scatter in magnitude but also to the slight differences in the sample selection with respect to the Petrosian LFs. This is, at least partially, behind the flattening of the faint-end slope in the $^{0.1}u$-band LF, where we have extended the apparent magnitude faint limit in almost 0.1 mag. As we have stressed several times throughout this work, the faint end of the bluer bands – especially the $^{0.1}u$ band – is extremely sensitive to variations of the faint limit of the sample, as a consequence of the large dispersion of the $^{0.1}u - {}^{0.1}r$ colour. Finally, and important for this work, the results shown in Fig. 15 seem to rule out the possibility that one of our most prominent findings, the so-called BEB, is an artefact caused by photometric errors.

3.3 Luminosity densities

To estimate the luminosity density, ρ, in all SDSS bands, we integrate throughout the entire absolute magnitude ranges defined by the limits shown in Table 5. In this table we list ρ in all bands obtained using the SWML estimate of the LFs shown in Figs 7 and 8. Luminosity densities are expressed in AB mag $(\mathrm{Mpc}^3\, h^{-3})^{-1}$. We also give in Table 5 the effective wavelength corresponding to each SDSS photometric band, $\lambda_{\rm eff}$. Errors shown in this table have been calculated using a similar bootstrapping technique as that discussed in Section 3.2. We have used 1000 random subsamples of 1/3 the number of objects in each sample.

As expected, the luminosity density in the nearby Universe increases with $\lambda_{\rm eff}$, in absolute values. This means that the Universe, up to $z \sim 0.2$, is considerably more luminous in the red side of the spectrum than it is in the blue side. Our luminosity densities obtained using the SWML estimate are in agreement with those from Blanton et al. (2003a) (see Table 5). Only in the $^{0.1}g$ band do discrepancies translate into a remarkable difference in the luminosity density. In this band, the nearby Universe is ∼0.8 mag brighter per unit volume, according to this work. In the rest of the bands, both estimates differ in ∼0.1 mag $(\mathrm{Mpc}^3\, h^{-1})^{-1}$, i.e. less than 1 per cent.

In Table 5, we also provide luminosity densities in each band obtained using the Schechter fits to the SWML estimates of the LFs presented in Section 3.2. As expected, the differences between these luminosity densities and those obtained with the SWML estimates are greater in the blue bands, where the Schechter LF provides a worse fit to our data points.

4 DISCUSSION

The main results presented in this work are the SDSS DR6 LFs of galaxies in the nearby Universe ($z = 0.1$). A few years ago, Blanton et al. (2003a) used an early version of the SDSS (DR2) to calculate the SDSS galaxy LFs. Now, with the SDSS DR6 available, galaxy statistics have improved by a huge factor of ∼7 in the very blue $^{0.1}u$ band and by a factor of between ∼3 and ∼5 in the rest of the SDSS photometric bands. Moreover, we have achieved a high-redshift completeness in our galaxy samples. First, we guarantee that the effect of brightness-dependent redshift incompleteness is small within the magnitude ranges that define our galaxy samples. Secondly, we ensure high completeness and avoid contamination from galaxies with $r > 17.6$ by means of carefully chosen apparent magnitude faint limits. These advances make our SDSS DR6 LFs substantially more precise than those from Blanton et al. (2003a) at both the bright and the faint ends. This said, the LFs of Blanton et al. (2003a) seem to be compatible with our results. However, notable differences, which are surely physically significant, exist. At the bright end of the blue bands LFs (especially in the $^{0.1}u$ band) we find a remarkable excess, which was very noisy in Blanton et al. (2003a) due to their lack of statistics. At the faint end, we obtain steeper slopes in all SDSS bands, especially in the $^{0.1}u$ band – where the DR6 statistics allow us to go about 0.5–1 mag deeper as compared to Blanton et al. (2003a) – and, in less extent, in the $^{0.1}g$ band.

With regard to the faint end of the LF, a possible explanation for these discrepancies – besides the consequence of the huge improvement in the galaxy statistics – could come from differences in the sample selections. It is well known that the faint end of the LF in the blue bands is very sensitive to variations of the flux limit of the sample, due to the large dispersion in the the $(g - r)$ and, especially, the $(u - r)$ colour. In Blanton et al. (2003a), the flux

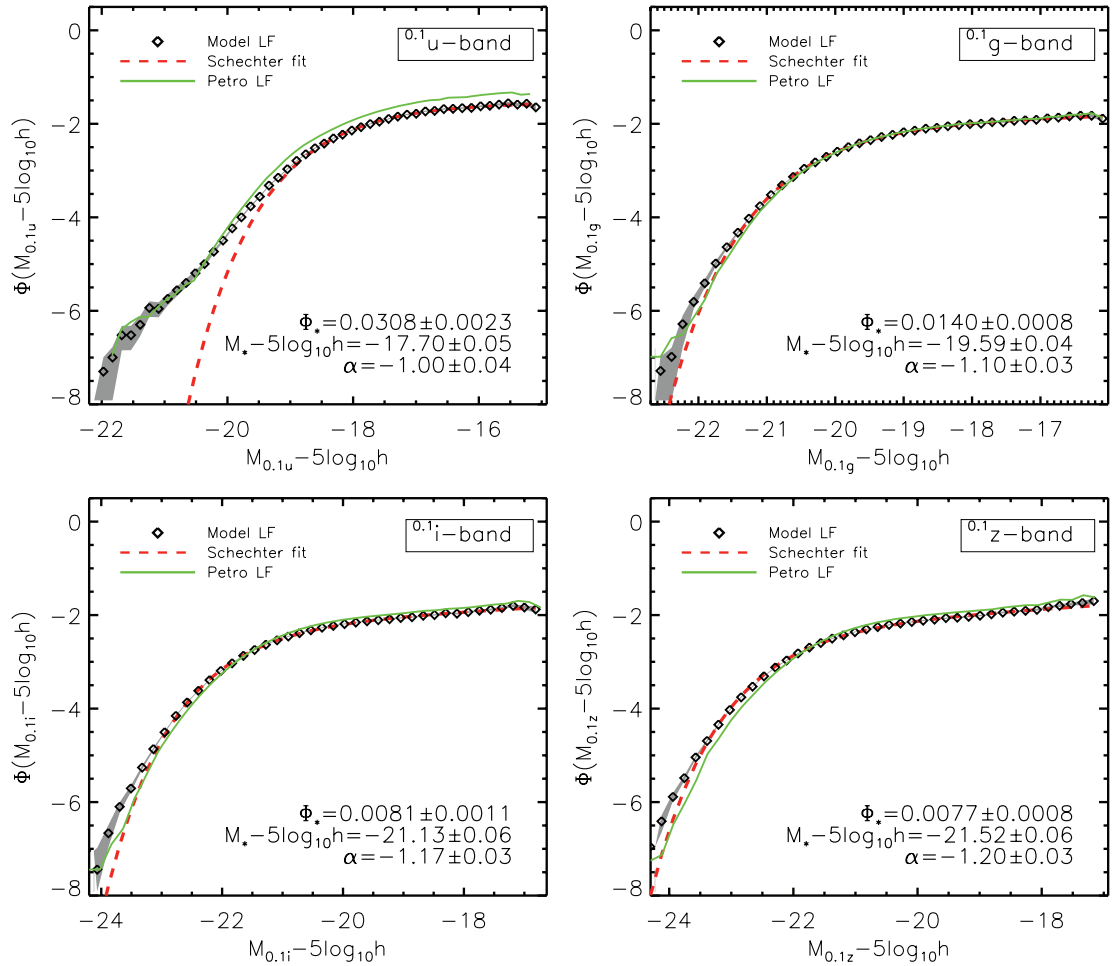

Figure 15. The SDSS DR6 LFs in bands $^{0.1}u$, $^{0.1}g$, $^{0.1}i$ and $^{0.1}z$ estimated using model magnitudes. SWML LF estimates are shown in diamonds and best-fitting Schechter functions are represented by dashed lines. In addition, we overplot in each panel the SDSS DR6 LF estimated using Petrosian magnitudes. Best-fitting values of Schechter parameters α, M_* and Φ_* are also shown. Shaded regions represent the 1σ uncertainty calculated using a bootstrapping technique.

Table 4. Values of Schechter parameters α, $M*$ and $\Phi*$ of the best-fitting Schechter function in all SDSS bands for the SDSS DR6 LF estimated using model magnitudes.

Band	Number	$m_{\rm min}$	$m_{\rm max}$	$z_{\rm min}$	$z_{\rm max}$	$\Phi*(10^{-2}\,h^3\,{\rm Mpc}^{-3})$	$M* - 5\log_{10}h$	α
u	159 018	16.45	18.90	0.020	0.170	3.07 ± 0.23	-17.70 ± 0.05	-1.00 ± 0.04
g	256 952	14.55	17.91	0.020	0.160	1.19 ± 0.08	-19.59 ± 0.04	-1.10 ± 0.03
r	466 280	13.93	17.6	0.020	0.220	0.78 ± 0.07	-20.83 ± 0.04	-1.24 ± 0.02
i	461 928	13.55	17.20	0.020	0.235	0.81 ± 0.11	-21.13 ± 0.03	-1.17 ± 0.03
z	422 643	13.40	16.85	0.020	0.240	0.77 ± 0.08	-21.52 ± 0.03	-1.20 ± 0.03

Table 5. Luminosity densities in AB mag $({\rm Mpc}^3\,h^{-3})^{-1}$ for all SDSS photometric bands calculated using the SWML estimate of the LFs of Figs 7 and 8 ($\rho_{\rm SWML}$) and the Schechter LF best fits of Table 2 ($\rho_{\rm Schechter}$). Absolute magnitude ranges of the integration and the effective wavelength corresponding to each band, $\lambda_{\rm eff}$, are also provided. Errors in $\rho_{\rm SWML}$ have been calculated using a bootstrapping technique. In addition, we give for comparison the luminosity densities from Blanton et al. (2003a).

Band	$\lambda_{\rm eff}$ (Å)	Absolute magnitude range	$\rho_{\rm SWML} + 2.5\log_{10}h$	$\rho_{\rm Schechter} + 2.5\log_{10}h$	$\rho_{\rm Blanton\,2003} + 2.5\log_{10}h$
$^{0.1}u$	3216	$-22.34 < M_{0.1u} < -15.11$	-14.009 ± 0.014	-14.377	-14.10 ± 0.15
$^{0.1}g$	4240	$-24.09 < M_{0.1g} < -16.01$	-14.386 ± 0.021	-14.783	-15.18 ± 0.03
$^{0.1}r$	5595	$-25.48 < M_{0.1r} < -16.32$	-15.814 ± 0.015	-15.803	-15.90 ± 0.03
$^{0.1}i$	6792	$-26.02 < M_{0.1i} < -16.72$	-16.355 ± 0.016	-16.138	-16.24 ± 0.03
$^{0.1}z$	8111	$-26.23 < M_{0.1z} < -17.05$	-16.661 ± 0.018	-16.491	-16.56 ± 0.02

limit is set at $u = 18.36$ and $g = 17.69$ in these bands, which means $\sim$0.5 and $\sim$0.2 mag brighter than in this work, respectively. This inconsistency could perfectly explain the discrepancies found in Fig. 8, as moving this limit towards brighter magnitudes produce a flattening of the faint-end slope. Even slight variations in the calculation of the LF itself could cause noticeable differences in these bands. Similarly, these inconsistencies could be responsible for the much smaller deviations that we find in the redder bands, where the LF is proved to be much more robust. In this sense, it is worth mentioning that relatively small variations in the shape of the LF may translate into considerable changes in the values of the best-fitting Schechter parameters. It is not convenient, therefore, to make comparisons between different LFs by just looking at these best-fitting Schechter parameters. Finally, we cannot neglect completely the effect of evolution in our galaxy samples, but as we have shown in Section 3.2.1, we expect it to be small enough not to change our faint-end slope significantly, given the uncertainties we are dealing with.

We have also seen that the BEB that we discovered in the blue bands (and also significantly in the $^{0.1}i$ band) is statistically very significant, according to our standard bootstrapping error analysis. Moreover, as we have mentioned previously, we also find clear – but noisy – evidence of its existence in Blanton et al. (2003a). We have also checked that this excess is not a consequence of any of the limits that we have imposed to define our samples. It is neither an artefact originated by photometric errors in Petrosian magnitudes nor a consequence of neglecting galaxy evolution within our redshift intervals. This is, therefore, a remarkable result that may have strong implications for galaxy evolution.

From a preliminary analysis on the nature of this BEB in the $^{0.1}u$-band LF, we have seen that it is mostly populated by SFs (including SBs) and active galaxies ($\sim$80 per cent). The spectra of these galaxies is consistent with what we expect from QSOs/type 1 Seyferts ($\sim$60 per cent) and SFs/SBs ($\sim$20 per cent). It seems, therefore, that an important fraction of the light that we receive from the brightest galaxies in the $^{0.1}u$ band would come from nuclear activity. Only about 20 per cent of galaxies in the BEB seem to be normal galaxies, showing no remarkable emission lines in their spectra.

Evidence of the existence of a similar BEB as the one discussed above has been found in the SAMs of galaxy formation by Croton et al. (2006). They report a bump at the bright end of the b_j-band LF of blue galaxies in their models (see their fig. 11). This excess is almost exclusively caused in the model by galaxies with very high star formation rates (SFRs) [note that active galactic nuclei (AGN) are not implemented in these models]. The authors conclude that these 'bump' galaxies are analogous to ultraluminous infrared galaxies (ULIRGs) and attribute the excess to an inadequate dust modelling within these objects. Despite the known limitations of these models, these results pose the question of whether a fraction of the SBs that we find among the BEBS galaxies are actually ULIRGs. We have seen, however, that SBs make a small contribution to the BEBS. A more detailed study is needed not only to answer this question but to fully understand the origin and the nature of the BEB galaxy population.

We note, finally, that we have not applied any correction for the light attenuation produced by dust inside each galaxy. Interstellar dust is known to have a strong impact on the flux of an individual galaxy, especially in the bluer bands, depending on the galaxy's inclination, bulge-to-total ratio and wavelength of observation (see Driver et al. 2007; Driver et al. 2008 for a realistic treatment of this issue). Correcting for this effect would therefore be necessary in any modelling that aims to constrain the stellar densities or the star formation histories of the Universe.

The implications of the new results presented in this paper could be investigated using SAMs of galaxy formation. With these models, we can, in principle, evaluate different processes and feedback relations that could reproduce our results.

5 SUMMARY

In this work we make use of the SDSS DR6 to estimate the number counts, LFs and luminosity densities of galaxies in all SDSS photometric bands. The SDSS DR6 is, by far, the most complete survey of the nearby Universe, containing redshifts for $\sim$1 000 000 galaxies down to magnitude $r \sim 17.77$ and covering $\sim$7400 deg^2 on the sky. The huge increase in the galaxy statistics with respect to the previous work of Blanton et al. (2003a) and the adequate treatment of brightness-dependent redshift incompleteness in our samples have allowed us to estimate the galaxy LFs of the nearby Universe with unprecedented accuracy. In addition, we have calculated, for the first time, the SDSS galaxy number counts in all photometric bands using spectroscopic data. Luminosity densities in all SDSS bands have also been computed.

The main results of this work can be summarized as follows.

(i) The SDSS DR6 galaxy number counts in all SDSS photometric bands are consistent with a Euclidean, non-evolving universe within a magnitude range that is limited by redshift incompleteness at the bright end and by the intrinsic apparent magnitude r-band limit of the survey at the faint end.

(ii) The SDSS DR6 LFs of galaxies are compatible with those of Blanton et al. (2003a). However, notable differences exist. At the bright end of the $^{0.1}u$-band LF we find a remarkable excess of $\sim$1.7 dex at $M_{^{0.1}u} \simeq -20.5$ with respect to the best-fitting Schechter LF. This BEB is very strong in the $^{0.1}u$ band and weakens in the $^{0.1}g$ band, fading away towards the very red $^{0.1}z$ band. At the faint end, we obtain steeper slopes in all bands, especially in the $^{0.1}u$ band and, in less extent, in the $^{0.1}g$ band. In addition, we can reach 0.5–1 mag deeper without losing precision.

(iii) We believe the discrepancies we find with respect to Blanton et al. (2003a) are primary due to the great increase in the sizes of the galaxy samples, of a factor of $\sim$7 in the $^{0.1}u$ band and between $\sim$3 and $\sim$5 in the rest of the SDSS bands, and to differences in the sample selection (especially in the lower limit in flux). We have also investigated the effect that accounting for galaxy evolution within our samples would have on our LFs. We have shown that, although it could produce slight adjustments to our LFs, it is unlikely to modify the main results presented in this work substantially.

(iv) A preliminary analysis of the origin of the BEB seen in the $^{0.1}u$-band SDSS DR6 LF reveals that it is composed of QSO and type 1 Seyferts galaxies ($\sim$60 per cent), SFs and SBs ($\sim$20 per cent) and normal galaxies ($\sim$20 per cent). It seems, therefore, that an important fraction of this exceeding luminosity might come from nuclear activity.

(v) We have estimated the SDSS DR6 LF using model magnitudes and found some clear differences with respect to the Petrosian LF. In the $^{0.1}u$ band, the faint-end slope of the LF flattens remarkably and, in the rest of the SDSS bands, the LF moves slightly to the bright end. These alterations are consistent with the scatter between model and Petrosian magnitudes in each band.

(vi) The $^{0.1}r$-band SDSS DR6 LF of blue galaxies is consistent with a Schechter LF with a remarkably steep faint-end slope, corresponding to $\alpha = -1.41$. The $^{0.1}r$-band SDSS DR6 LF of red galaxies

has, however, a slightly decreasing faint-end slope, corresponding to $\alpha = -0.81$.

(vii) The SDSS DR6 luminosity densities of galaxies are in very good agreement with Blanton et al. (2003a) in bands $^{0.1}u$, $^{0.1}r$, $^{0.1}i$ and $^{0.1}z$. In the $^{0.1}g$ band, however, we find that the Universe in the redshift range considered is $\sim$0.8 mag brighter per unit volume.

The state-of-the-art results presented in this paper may be used to constrain a variety of aspects of star formation histories or feedback processes in galaxy formation models. However, much effort is still needed in the survey field to fully understand the mechanisms that drive the evolution of galaxies in the Universe. This is especially necessary at high z, where statistics are still very poor.

ACKNOWLEDGMENTS

ADM-D is supported by the Ministerio de Educación y Ciencia of the Spanish Government (MEC) through FPI grant AYA2005-07789. ADM-D and FP acknowledge the MEC for their financial support through PNAYA2005-07789.

We thank the anonymous referee for helpful suggestions, which improved the content, clarity and presentation of this paper.

We would like to especially thank Michael Blanton for providing help on the calculation of the LF and giving comments on the manuscript. We acknowledge Michael Blanton and David Hogg as the corresponding authors of the NYU-VAGC DR6.

We also thank Jonatan Hernández-Fernández, Víctor M. Muñoz Marín, Darren Croton, Anatoly Klypin, Simon White, Alister Graham, Sandy Faber, Santiago Patiri and Hans-Walter Rix for stimulating scientific discussions. Finally, we thank Antonio J. Cuesta for providing technical help throughout the process of making this work.

Funding for the SDSS has been provided by the Alfred P. Sloan Foundation, the Participating Institutions, NASA, the NSF, the US Department of Energy, the Japanese Monbukagakusho and the Max Planck Society. The SDSS website is http://www.sdss.org/.

REFERENCES

Adelman-McCarthy J. K. et al., 2008, ApJS, 175, 297
Blanton M. R. et al., 2001, AJ, 121, 2358
Blanton M. R. et al., 2003a, ApJ, 592, 819
Blanton M. R. et al., 2003b, ApJ, 594, 186
Blanton M. R., Lupton R. H., Schlegel D. J., Strauss M. A., Brinkmann J., Fukugita M., Loveday J., 2005a, ApJ, 631, 208
Blanton M. R. et al., 2005b, AJ, 129, 2562
Colless M. et al., 2001, MNRAS, 328, 1039
Corwin H. G., Jr, Buta R. J., de Vaucouleurs G., 1994, AJ, 108, 2128
Croton D. J. et al., 2006, MNRAS, 365, 11
da Costa L. N. et al., 1988, ApJ, 327, 544
Davis M., Huchra J., 1982, ApJ, 254, 437
Davis M., Efstathiou G., Frenk C. S., White S. D. M., 1985, ApJ, 292, 371
Davis M. et al., 2003, Proc. SPIE, 4834, 161
Driver S. P., Popescu C. C., Tuffs R. J., Liske J., Graham A. W., Allen P. D., de Propris R., 2007, MNRAS, 379, 1022
Driver S. P., Popescu C. C., Tuffs R. J., Graham A. W., Liske J., Baldry I., 2008, ApJ, 678, L101
Drory N., Feulner G., Bender R., Botzler C. S., Hopp U., Maraston C., Mendes de Oliveira C., Snigula J., 2001, MNRAS, 325, 550
Efstathiou G., Ellis R. S., Peterson B. A., 1988, MNRAS, 232, 431
Feulner G., Goranova Y., Hopp U., Gabasch A., Bender R., Botzler C. S., Drory N., 2007, MNRAS, 378, 429
Giovanelli R., Haynes M. P., 1991, ARA&A, 29, 499
Huchra J., Davis M., Latham D., Tonry J., 1983, ApJS, 52, 89
Humason M. L., 1956, Vistas Astron., 2, 1620
Khochfar S., Silk J., Windhorst R. A., Ryan R. E., Jr, 2007, ApJ, 668, L115
Le Fevre O. et al., 2003, Proc. SPIE, 4834, 173
Marzke R. O., Huchra J. P., Geller M. J., 1994, ApJ, 428, 43
Norberg P. et al., 2002, MNRAS, 336, 907
Petrosian V., 1976, ApJ, 210, L53
Sandage A., 1978, AJ, 83, 904
Schechter P., 1976, ApJ, 203, 297
Shapley H., Ames A., 1932, Ann. Harv. Coll. Obser., 88, 41
Shectman S. A., Landy S. D., Oemler A., Tucker D. L., Lin H., Kirshner R. P., Schechter P. L., 1996, ApJ, 470, 172
Springel V. et al., 2005, Nat, 435, 629
Stoughton C. et al., 2002, AJ, 123, 485
Strateva I. et al., 2001, AJ, 122, 1861
Strauss M. A. et al., 2002, AJ, 124, 1810
Yasuda N. et al., 2001, AJ, 122, 1104
York D. G. et al., 2000, AJ, 120, 1579

This paper has been typeset from a TEX/LATEX file prepared by the author.